Effects of rescattering in $(e,e'p)$ reactions within a semiclassical model

C. Barbieri*

TRIUMF, 4004 Wesbrook Mall, Vancouver, British Columbia, Canada V6T 2A3

L. Lapikás

Nationaal Instituut voor Kernfysica en Hoge-Energiefysica (NIKHEF), P.O. Box 41882, 1009 DB Amsterdam, The Netherlands

The contribution of rescattering to final state interactions in $(e,e'p)$ cross sections is studied for medium and high missing energies using a semiclassical model. This approach considers two-step processes that lead to the emission of both nucleons. The effects of nuclear transparency are accounted for in a Glauber-inspired approach and the dispersion effects of the medium at low energies are included. It is found that rescattering is strongly reduced in parallel kinematics. At high missing energies and momenta, the distortion of the short-range correlated tail of the spectral function is dominated by a rearrangement of that strength itself. In perpendicular kinematics, a further enhancement of the experimental yield is due to strength that is originally in the mean field region. This contribution becomes negligible at large missing momenta.

I. INTRODUCTION

Nuclear correlations strongly influence the dynamics of nuclear systems [1,2]. In particular, the repulsive core at small internucleon distances has the effect of depleting the shell model orbitals and inducing high momentum components in the nuclear wave functions [3,4]. The main effects of short-range correlations (SRC) consist of shifting a sizable amount of spectral strength, about 10–15 % [5], to very high missing energies and momenta, together with increasing the binding energy [6]. The resulting reduction of the occupation numbers of the deeply bound orbitals appears to be fairly independent of the given subshell and of the size of the nucleus, except for a slight increase with the central density of the system. Theoretical studies of the distribution of short-range correlated nucleons for finite nuclei have been carried out using a local density approximation (LDA) by Benhar *et al.* [7] and with many-body Green's functions by Müther *et al.* [3]. These calculations suggest that most of the missing strength is found along a ridge in the momentum-energy plane $(p_m\text{-}E_m)$, which spans several hundreds of MeV/c (and MeV). Such behavior is confirmed by recent experimental data [8].

It is important to note that the depletion of spectroscopic factors for closed shell orbitals observed near the Fermi energy is more substantial than the 15% reduction discussed above [9] due to long-range effects such as the coupling to collective modes [2]. We note that this reduction also tends to be weaker for loosely bound orbitals such as halo states [10,11]. As a consequence, it becomes particularly interesting to study the spectral distribution in heavy nuclei where the mean field single-particle orbitals extend to regions far from the Fermi level and tend to decouple from surface effects. A measurement of the spectral function for the complete mean field region of ^{208}Pb has been undertaken recently

at NIKHEF [12]. In this region the single-particle orbitals are sensibly fragmented and it is required to probe missing energies up to 100 MeV [12] or more. Further detailed information on SRC could be obtained from $(e,e'p)$ experiments that directly search for the missing strength at very high missing momenta and energies. This is particularly appealing since the details of its distribution strongly influence the binding energy of finite nuclei and nuclear matter [6]. Besides, it could shed more light on how much the interior of large nuclei is sensitive to the effects of finite size and proton-neutron asymmetry.

Unfortunately, past measurements of the short-range correlated tail by means of $(e,e'p)$ reactions have been limited due to the enormous background that is generated by final state interactions (FSI) (see, for example, Refs. [13,14]). The issue of how to minimize the FSI has been recently addressed in Ref. [15]. There, it was suggested that FSI in exclusive $(e,e'p)$ cross sections are dominated by two-step rescattering processes like the one depicted in Fig. 1. This becomes particularly relevant when regions of small spectral strength are probed in perpendicular kinematics.[1] A study of several kinematic conditions shows that the rescattered nucleons can move spectral strength in the $p_m\text{-}E_m$ plane, from the top of the ridge toward regions where the correlated strength is small, therefore submerging the direct signal in a large background noise. Other possible contributions that involve the excitation of a Δ resonance are expected to be more sensitive to transverse degrees of freedom. Parallel kinematics tend to be more clean due to the high momentum that is required for the detected proton. In Ref. [15], it was suggested that the contribution of rescattering can be diminished by choosing parallel kinematics and taking advantage of modern electron beam facilities. New data were subse-

---

[1]In this work we refer to "parallel" and "perpendicular" kinematics in terms of the angle between the momentum of the virtual photon $\mathbf{q}$ and the missing momentum $\mathbf{p}_m$ (as opposed to the outgoing proton $\mathbf{p}_f$).
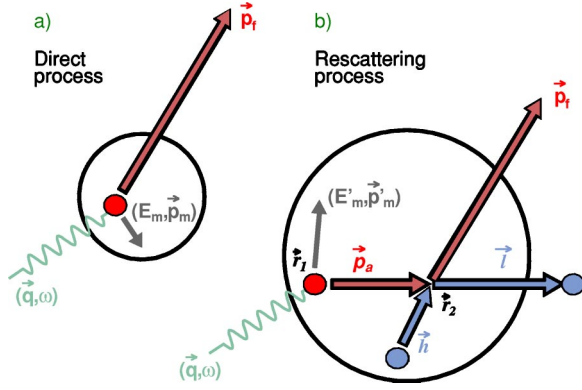
*Electronic address: barbieri@triumf.ca

FIG. 1. (Color online) Schematic representation of the direct knockout of a proton (a), given by the plane wave impulse approximation, and the contribution from a two-step rescattering (b). In the latter a proton or neutron is emitted with momentum $\mathbf{p}_a$ and different missing energy and momentum $(E'_m, \mathbf{p}'_m)$. Due to a successive collision, a proton is eventually detected with the same momentum $\mathbf{p}_f$ seen in the direct process.

quently taken in these conditions by the E97-006 collaboration at Jefferson Laboratory [8,16,17] for a set of nuclei ranging from carbon to gold. Clearly, FSI could still play a role even in parallel kinematics and need to be properly addressed before the relevant physical information is extracted from the experiment. We note that a similar dependency of the FSI on the kinematics is also predicted in Ref. [18] for $(e,e'NN)$ reactions in superparallel kinematics.

The issue of computing the effects of rescattering has been considered recently by means of the multistep dynamics approach [19] and by using Glauber theory [20–22]. All these calculations suggest that multiple rescattering contributions (more than two steps) are relatively small in light nuclei like ^{12}C but can become relevant for large systems. Interference effects between FSI and SRC correlations can also play a role [21]. However, all these effects were seen to be reduced in parallel kinematics. In Ref. [12], the scattered proton was detected at energies at which a full distorted wave calculation, in terms of an optical potential, is required. However, rescattering processes leading to the emission of two nucleons (one of which is not detected) can lead to the reappearance of a part of the experimental strength absorbed by inelastic processes. This effect was investigated in terms of a semiclassical model inspired by the work of Ref. [23]. Even if very different kinematical situations were considered, the reaction mechanism included in the latter approach is the same as pointed out in Ref. [15] and Fig. 1. Some partial simplifications occur for high-energy protons, since the relevant effects of the medium are limited to Pauli blocking. Therefore this approach offers a valid starting point to investigate the FSI effects needed in the analysis of data at large missing energy and momenta. Other effects such as meson exchange currents and the excitation of resonances also need to be investigated. However, these are beyond the scope of the present paper and will be considered in future work. In this paper, we consider the approach of Ref. [12] and extend it to high missing energies. We then apply it to the kinematics of both the NIKHEF [12] and the E97-006

[16,17] experiments to evaluate the importance of two-step processes for the different kinematics employed.

The model for computing the contribution of rescattering is depicted in Sec. II, together with a discussion of the inclusion of the absorption effects in terms of nuclear transparency. A practical application requires the knowledge of the in-medium differential cross section, which is calculated in Sec. III by extending the approach of Ref. [23]. Sections IV A and IV B report on the results for the kinematics used in the above experiments at medium and high missing energies, respectively. Conclusions are drawn in Sec. V.

II. MODEL

This work considers contributions to the experimental yield that come from two-step mechanisms in which a reaction $(e,e'a)$ is followed by a scattering process from a nucleon in the medium, $N'(a,p)N''$, eventually leading to the emission of the detected proton. In general, a may represent a nucleon or another possible intermediate particle. In this work we will only consider the channels in which a is either a proton (with $N'=p$ or n) or a neutron. In the following we will also use the letter a to label the possible open channels.

Following the semiclassical approach of Refs. [12,23], the contribution to the cross section coming from rescattering through the above channels is written as

$$\frac{d^6\sigma_{rescatt}}{dE_0 d\Omega_{\hat{k}_o} dE_f d\Omega_{\hat{p}_f}}$$

$$= \sum_a \int d\mathbf{r}_1 \int d\mathbf{r}_2 \int_0^\omega dT_a \rho_N(\mathbf{r}_1)$$

$$\times \frac{K\, S_a^h(p'_m, E'_m)\sigma_{ea}^{cc1}}{M(\mathbf{r}_1 - \mathbf{r}_2)^2} g_{aN'}(|\mathbf{r}_1 - \mathbf{r}_2|)$$

$$\times P_T(p_a; \mathbf{r}_1, \mathbf{r}_2)\rho_{N'}(\mathbf{r}_2)\frac{d^3\sigma_{aN'}}{dE_f d\Omega_{\hat{p}_f}}P_T(p_f; \mathbf{r}_2, \infty), \quad (1)$$

where $(E_o, \mathbf{k}_o)$ and $(E_f, \mathbf{p}_f)$ represent the four-momenta of the detected electron and proton, respectively. Equation (1) assumes that the intermediate particle a is generated in plane wave impulse approximation (PWIA) by the electromagnetic current at a point $\mathbf{r}_1$ inside the nucleus. Here $K=|\mathbf{p}_a|E_a$ is a phase space factor, $S_a^h(p'_m, E'_m)/M$ is the spectral function of the hit particle a normalized to one [i.e., $M=N\,(Z)$ if a is a neutron (proton)], and σ_{ea}^{cc1} the off shell electron-nucleon cross section, for which we have used the $cc1$ prescription of de Forest [24]. The pair distribution functions $g_{aN'}(|\mathbf{r}_1 - \mathbf{r}_2|)$ account for the joint probability of finding a nucleon N' in $\mathbf{r}_2$ after the particle a has been struck at $\mathbf{r}_1$ [25]. The integration over the kinetic energy T_a of the intermediate particle a ranges from 0 to the energy ω transferred by the electron. The nuclear transparency factor $P_T(p; \mathbf{r}_1, \mathbf{r}_2)$ gives the transmission probability that the struck particle a propagates, without any interactions, to a second point $\mathbf{r}_2$, where it scatters from the nucleon N' with cross section $d^3\sigma_{aN'}$. The whole process is depicted in Fig. 1(b). The point nucleon densities $\rho_N(\mathbf{r})$ are normalized to either the number of neutrons or protons.

These were derived from experimental charge distributions by unfolding the proton size [26]. We employed equal distributions for neutrons and protons, which is a sufficiently accurate approximation since even in ^{208}Pb neutron and proton radii differ by less than 4%.

The nuclear transparency for the ejected nucleon was considered in Ref. [23] according to Glauber theory. The probability P_T that a proton struck at $\mathbf{r}_1$ will travel with momentum $\mathbf{p}$ to the point $\mathbf{r}_2$ without being rescattered is given by

$$P_T(p;\mathbf{r}_1,\mathbf{r}_2) = \exp\left\{ -\int_{z_1}^{z_2} dz[g_{pp}(|\mathbf{r}_1-\mathbf{r}|)\tilde{\sigma}_{pp}(p,\rho(\mathbf{r}))\rho_p(\mathbf{r}) \right.$$
$$\left. + g_{pn}(|\mathbf{r}_1-\mathbf{r}|)\tilde{\sigma}_{pn}(p,\rho(\mathbf{r}))\rho_n(\mathbf{r})] \right\}, \quad (2)$$

where the z axis is chosen along the direction of propagation $\hat{\mathbf{p}}$, an impact parameter $\mathbf{b}$ is defined so that $\mathbf{r}=\mathbf{b}+z\hat{\mathbf{p}}$, and $z_1(z_2)$ refers to the initial (final) position. Equation (2) differs from the standard Glauber theory by the inclusion of the pair distribution functions $g_{pN}(|\mathbf{r}_1-\mathbf{r}|)$. In principle, the g_{pN} functions should depend on the density and on the direction of the interparticle distance. However, these effects have been shown to be negligible in Ref. [23]. In the present application we find that a simple two-Gaussian parametrization of the g_{pN} can adequately fit the curves reported there for nuclear matter at saturation density. The in-medium total cross sections $\tilde{\sigma}_{pp}(p,\rho)$ and $\tilde{\sigma}_{pn}(p,\rho)$ used in this work have been computed according to Ref. [23] and account for the effects of Pauli blocking, Fermi spreading, and the effective mass generated by the nuclear mean field. For energies above 300 MeV they have been extended to incorporate the effects of pion emission [27].

The nuclear transparency is defined as the average over the nucleus of the probability that the struck proton emerges from the nucleus without any collision. This is related to P_T by

$$T = \frac{1}{Z}\int d\mathbf{r}\,\rho_p(\mathbf{r})P_T(p;\mathbf{r},\infty). \quad (3)$$

It should be mentioned that the practical experimental definition of nuclear transparency depends on the specific kinematics employed and that Eqs. (2) and (3) rigorously apply only to the parallel case [28]. For the present approach, these are the right quantities to be included in Eq. (1) since they describe the loss of flux in the direction of propagation. In the case of ^{208}Pb and an outgoing proton with energy $E_f \sim 1.1$ GeV (kinetic energy of ~ 161 MeV), Eq. (3) gives $T = 0.37$. With $E_f \sim 1.8$ GeV, which is of interest for the calculations of Sec. IV B, $T=0.63$ for ^{12}C and $T=0.29$ for ^{197}Au. The PWIA contribution of the direct process, Fig. 1(a), also needs to be corrected for the nuclear transparency effects,

$$\frac{d^6\sigma_{\mathrm{PWIA}(T)}}{dE_0 d\Omega_{\hat{k}_o} dE_f d\Omega_{\hat{p}_f}} = K\sigma_{ep}^{cc1}S_p^h(p_m,E_m)T, \quad (4)$$

with T given by Eq. (3). Equation (4) is consistent with the assumptions of Eq. (1), from which it would be obtained if

the rescattering event was substituted with the limit of $\mathbf{r}_2$ to infinity.

III. EVALUATION OF THE IN-MEDIUM NUCLEON-NUCLEON RATE

The last ingredient required in Eq. (1) is the in-medium cross section for the rescattering process, in which the particle a (either a proton or a neutron) hits against a bound nucleon on its way out, eventually leading to the emission of the detected proton. This can be evaluated by extending the approach of Ref. [23] to describe the angular dependence of the ejected proton. We start from the NN differential elastic cross section in free space,

$$\frac{d\sigma_{pN}}{d\Omega_{\hat{p}_f}} = |f_{pN}(\cos\theta)|^2 = \frac{|\bar{\mathcal{M}}(s,t,u)|^2}{64\pi^2 s}, \quad (5)$$

where s, t, and u are the Mandelstam invariants [$\sqrt{s}$ being energy in the center of mass (c.m.) system] and $|\bar{\mathcal{M}}(s,t,u)|^2$ represents the square of the Lorentz invariant amplitude [29] averaged (summed) over the initial (final) spins. For nucleon momenta above 1 GeV/c and for small angles, the scattering amplitude in Eq. (5) is well approximated by its central part and can be written as

$$f_{pN} = \frac{p_f\sigma_{pN}^{tot}}{4\pi}(\epsilon_{pN}+i)\exp\{-\beta_{pN}^2(\mathbf{p}_i-\mathbf{p}_f)^2/2\}, \quad (6)$$

where $\mathbf{p}_i$ and $\mathbf{p}_f$ are the initial and final momenta of the scattered nucleon, ϵ_{pN} is the ratio of the real to imaginary part of the scattering amplitude, and σ_{pN}^{tot} is the total scattering cross section. At low energy the values of $\mathcal{M}(s,t,u)$ where extracted from the SAID phase shift data analysis [30]. For the pp case, we chose to keep the differential cross section constant for angles smaller than 5° and larger than 175°, in order to avoid the Coulomb peak in the forward and backward directions. However, the results of the present work are largely insensitive to this choice of the cutoff angle due to Pauli exclusion. The solutions of the SAID program were used for energies in the laboratory system up to 1.6 GeV for pp scattering and 1.2 GeV for the pn case, which are well contained within the range of validity of this database. At higher energies Eq. (6) was used with parameters $\sigma_{pp}^{tot}=44.0$ mb, $\sigma_{pn}^{tot}=41.1$ mb, and $\epsilon_{pp}=\epsilon_{pn}=-0.48$. The slope coefficients were chosen by requiring that Eq. (5) yields the correct values σ_{pN}^{el} for the total elastic cross section. This implies

$$\beta_{pN}^2 \simeq \frac{(1+\epsilon_{pN}^2)\sigma_{pN}^{tot^2}}{16\pi\sigma_{pN}^{el}}, \quad (7)$$

where σ_{pp}^{el} and σ_{pn}^{el} were extracted from experiment [31]. A direct comparison for energies above 1 GeV showed that Eq. (6) appropriately approximates the data from the SAID database; thus there exists an overlap region where these approaches are both accurate and join smoothly.

In deriving the rescattering rate we assume that the interaction between the two nucleons is localized enough so that

the amplitude $\mathcal{M}(s,t,u)$ is not altered by the presence of the surrounding nucleons. However, the medium can sensibly modify the cross section due to the spectral distribution of the momentum of the hit nucleon and due to the effects of Pauli blocking. In the spirit of the LDA, which underlies Eq. (1), the momentum of the hit nucleon, N', is taken to be locally distributed as in infinite nuclear matter. The density of the latter being the one of point $\mathbf{r}_2$ where the collision occurs, $\rho_{NM}=\rho_{N'}(\mathbf{r}_2)$. The effects of the nuclear surface are eventually included by integrating over $\rho_{N'}(\mathbf{r}_2)d\mathbf{r}_2$ in Eq. (1). For the present purposes it is appropriate to further approximate the symmetric nuclear matter with a free Fermi gas.[2] The assumption of a completely filled Fermi sea is also consistent with the Dirac-Brueckner-Hartree-Fock (DBHF) employed below. Initially, the hit nucleon N' is in the Fermi sea and therefore must have a momentum $\mathbf{h}$ smaller than k_F $=(3\pi^2\rho_{NM}/2)^{1/3}$. At the same time the Pauli principle requires that the particles in the final state will have momenta $\mathbf{p}_f$ and $\mathbf{l}$, both larger than k_F. Among all the nucleons involved in the process, $\mathbf{p}_f$ refers to the detected proton while the others can be either neutrons or protons depending on the channel a. The probability per unit time of an event leading to the emission of a proton with momentum $\mathbf{p}_f$ is obtained by imposing the Pauli constraints and integrating over the unobserved momenta $\mathbf{h}$ and $\mathbf{l}$,

$$
\begin{aligned}
\frac{d^3P_{aN'}}{dp_f d\Omega_{\hat{p}_f}} &= 2\ \theta(p_f-k_F)L^3 \int\int \frac{d\mathbf{h}\,d\mathbf{l}}{(2\pi)^6}\theta(k_F-h)\,\theta(l-k_F)W_I \\
&= 2\ p_f^2\theta(p_f-k_F)\int\frac{d\mathbf{h}}{(2\pi)^3}\theta(k_F-h)\,\theta(l-k_F) \\
&\quad\times\left|\frac{1}{64\pi^2}\frac{|\bar{\mathcal{M}}(s,t,u)|^2}{E_a(p_a)E_{N'}(h)E_f(p_f)E_{N''}(l)}\right. \\
&\quad\left.\times\delta(E_a+E_{N'}-E_f-E_{N''})\right|_{\mathbf{l}=\mathbf{p}_a+\mathbf{h}-\mathbf{p}_f}
\end{aligned}
\tag{8}
$$

where L^3 is the volume of a normalization box and, for a free nucleon, $E_N(p)=(p^2+m_N^2)^{1/2}$. In Eq. (8), W_I is the probability per unit time for the event $p_a^\mu+h^\mu\rightarrow p_f^\mu+l^\mu$, which can be expressed in terms of $\mathcal{M}(s,t,u)$. The inverse lifetime of the nucleon a for energies below the pion production threshold is related to Eq. (8) by

$$
\frac{1}{\tau_a}=\sum_{N'=p,n}\int d\Omega_{\hat{p}_f}\int dp_f\frac{d^3P_{aN'}}{dp_f d\Omega_{\hat{p}_f}}.
\tag{9}
$$

At low energies, a nucleon traveling through the medium acquires an effective mass due to dispersion effects. For infinite matter, this can be described by a scalar field U_S and the time component of a vector field U_V [32]. This particular

[2]Note that in correlated nuclear matter a sizable number of protons ($\sim 15\%$) have momentum larger than k_F. However, the error on the spreading effects generated by considering all of them inside the Fermi sea did not appear to be relevant in Ref. [12]. This discrepancy also tends to reduce further for large nucleon energies.
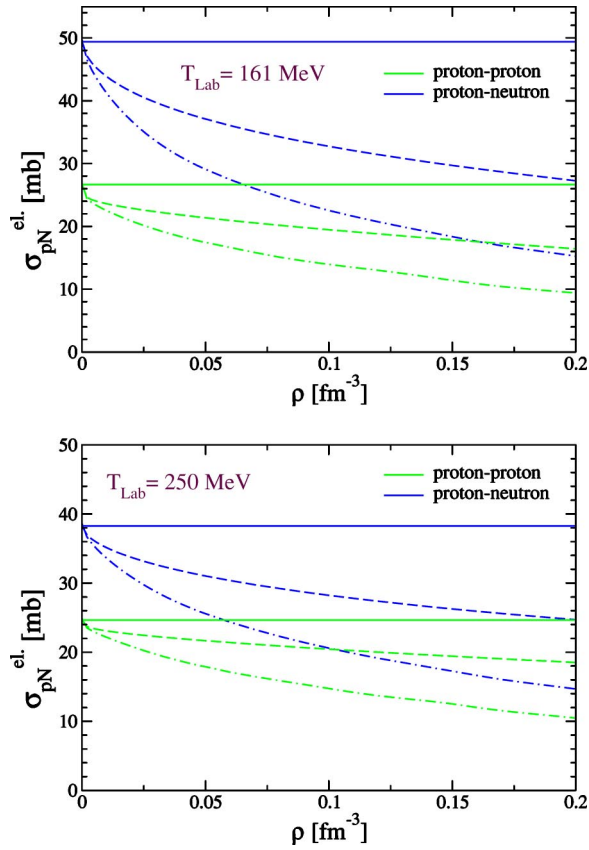
approach allows us to maintain the relativistic framework adopted in Eq. (8). The values of U_S and U_V in nuclear matter were computed in Ref. [33] by solving the DBHF equations. The results were found to be consistent with the value of the nonrelativistic effective mass extracted from nucleon-nucleus scattering. At the energies considered by the DBHF calculations, U_S and U_V are predicted to be essentially momentum independent. Thus, the energy of a nucleon moving with momentum p is given by

$$
m_D(\rho_{NM})=m_N+U_S(\rho_{NM}),
\tag{10}
$$

$$
E_N(p,\rho_{NM})=\sqrt{p^2+m_D^2(\rho_{NM})}+U_V(\rho_{NM}),
\tag{11}
$$

where m_D is the Dirac effective mass. It should be noted that U_S and U_V have large and opposite values. The success of the DBHF approach relies on a subtle cancellation of their effects and require a self-consistent calculation of the interaction with the medium [33]. As a consequence, the use of Eqs. (10) and (11) to compute the in-medium cross section at low energy does not guarantee *a priori* accurate predictions. In a relativistic model, this would require a more elaborate calculation of the scattering amplitude $\mathcal{M}$ (see, for example, Refs. [34,35]). In the present work, we are simply interested in giving an approximate treatment of the dispersion effects on the rescattering of protons for the kinematics that will be considered in Sec. IV A. The kinematics relevant for studying the short-range correlated tail involve much higher energies, where the nuclear cross section is known to approach the free one. Above 1 GeV, U_S and U_V are not known except that they are no longer momentum independent and that they should decrease to zero. In this case, Pauli blocking gives the only relevant contribution of the medium and the dispersion effects are negligible. Therefore U_S and U_V will be set to zero in the calculations of Sec. IV B.

When the effective mass is accounted for, the momentum of a nucleon participating in the rescattering process is related to its energy $E(p)$ by Eq. (11). In general, $\mathcal{M}(s,t,u)$ is off shell. However, following the assumption that the interaction is not appreciably modified by the in-medium effects we use the on-shell values extracted from the vacuum pN cross section, Eq. (5). In vacuum, this depends on only two invariants that were chosen to be $s=(p_a^\mu+h^\mu)^2$ and $t=(p_a^\mu-p_f^\mu)^2$ and computed accounting for the dispersion relation (11). The energy denominators appearing in Eq. (8) were also taken to be equal to the total energy of the nucleon, Eq. (11). We note that this differs from the normalization of a Dirac spinor in the medium [32]. However, this prescription is consistent with the choice of using the free scattering amplitude $\mathcal{M}(s,t,u)$ since it provides the right normalization in the nonrelativistic limit. Finally, the in-medium scattering rate is given by

$$
\frac{d^3\sigma_{aN'}}{dE_f d\Omega_{\hat{p}_f}}=\frac{1}{\rho_{N'}v_g}\frac{dp_f}{dE_f}\frac{d^3P_{aN'}}{dp_f d\Omega_{\hat{p}_f}},
\tag{12}
$$

where $\rho_{N'}$ is the density of the hit nucleon and v_g $=dE_a(p_a)/dp_a=p_a/\sqrt{p_a^2+m_{Da}^2}$ is the group velocity of the incoming one. Note that the dispersion effects modify the rescattering rate, Eq. (12), in three different ways. First, both v_g

FIG. 3. (Color online) In medium elastic pN cross sections computed for normal nuclear matter density as a function of the nucleon energy. The curves show the vacuum cross section (full line), the results obtained by including Pauli blocking and Fermi spreading (dashed line) and also the dispersion effects (dot-dashed line).

FIG. 2. (Color online) In-medium elastic pN cross sections as a function of density for laboratory energies of 161 MeV (top panel) and 250 MeV (bottom panel). The curves show the vacuum cross section (full line), the results obtained by accounting for Fermi spreading and Pauli blocking (dashed line) and by adding the interaction with the medium through Eq. (11) (dot-dashed line).

and the Jacobian dp_f/dE_f depend on U_S and U_V. Second, the density of final states for the scattered nucleons is modified by using Eq. (11) in the energy delta function $\delta(E_a(p_a) + E_{N'}(h) - E_f(p_f) - E_{N''}(l))$. Third, the energies of nucleons just above k_F are lowered by Eq. (11), which allows scattering at energies that would otherwise be Pauli forbidden.

Figure 2 shows the in-medium effective cross section as a function of density obtained by integrating Eq. (12) over angle and energy. Two values of the energy of the incoming nucleon are considered. The solid line gives the vacuum cross section while the dashed line includes the effects of Pauli blocking and Fermi spreading. A further reduction is produced by accounting for the dispersion effects. While the calculation of the Pauli blocking effects is equivalent to the work of Ref. [23], the full cross section obtained here is somewhat smaller than the one obtained in the corresponding nonrelativistic result. A difference between the two approaches should be expected since the present calculation is based on the Dirac effective mass, given by Eq. (10). This is different form the nonrelativistic definition of effective mass, which is instead related to the vector potential U_V [36]. The effects of Pauli blocking at higher energies can be seen in Fig. 3 where the elastic cross section is computed at normal
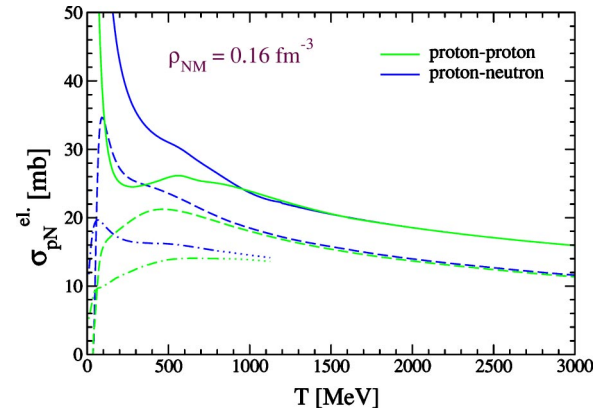
nuclear matter density $\rho_{NM}=0.16$ fm^{-3} for energies up to 3 GeV. As it can be seen, the effects of Pauli blocking remain relevant at large energies where they produce a constant reduction of the cross section. The further reduction due to the effective mass affects the results at low energies and tends to become less important at 1 GeV even for constant values of U_S and U_V. However, it is meaningless to extend the calculation of the effective mass effects above this energy since the values of U_S and U_V are unknown in this region.

IV. RESULTS

Equation (1) requires the knowledge of the undistorted spectral function $S^h(p_m,E_m)$ of the target nucleus. For the present purposes, the strength in the mean field region can be described as a sum over the nuclear orbitals

$$S^h_{MF}(p_m,E_m) = \sum_i Z_i f_i(E_m)|\Phi_i(p_m)|^2, \qquad (13)$$

where $\Phi_i(p_m)$ are the single-particle wave functions, Z_i are their occupation numbers, and each orbital is spread in energy according to a Lorentzian distribution with a variable width [37],

$$f_i(E_m) = \frac{1}{2\pi}\frac{\Gamma(E_m)}{(E_m - \varepsilon_i)^2 + [\Gamma(E_m)/2]^2}, \qquad (14)$$

$$\Gamma(E_m) = \frac{a(E_m - E_F)^2}{b + (E_m - E_F)^2}, \qquad (15)$$

where the Fermi energy was taken to be $E_F=6$ MeV, $a=24$ MeV, and $b=500$ MeV^2. The neutron spectral function was also obtained from Eq. (13) by including all the neutron orbits occupied in the shell structure. For Pb and Au no experimental data are available for neutrons, thus the occupation numbers Z_i were assigned by extrapolating the trend measured for protons in ^{280}Pb [12]. For kinematics chosen to probe medium and low missing energies, as those discussed in Sec. IV A, $S^h_{MF}(p_m,E_m)$ covers all experimentally acces-

sible strength. In Sec. IV B, this will need to be extended by including the distribution of nucleons in the SRC correlated region.

In the following, the rescattering yield computed from Eq. (1) has been converted to a reduced spectral function by dividing it by $|p_f E_f| T \sigma_{eN}^{cc1}$, evaluated for the kinematics of the direct process [according to Eq. (4)]. This gives the straight-forward correction to the model spectral function that is due only to single rescattering effects.

A. Application to ^{208}Pb

The studies of Ref. [12] employed two different parallel kinematics in which the outgoing proton was emitted in the same direction as the momentum transfer (thus **q** and **p**$_m$ were also parallel). The central kinetic energy of the outgoing proton was kept constant at 161 MeV ($p_f = 570$ MeV/c) in both cases. The two kinematics differ only for the energy of the electron beam, which was taken to be $E_o^H = 674$ MeV for the first case and $E_o^L = 461$ MeV for the other. These choices correspond to a virtuality Q^2 ranging between 0.08 and 0.22 GeV^2.

In applying the model of Secs. II and III to $(e, e'p)$ reactions one has to impose the further constraint that both nucleons are emitted in the continuum. This is trivially satisfied for high-energy nucleons, for which the interaction with the medium can be neglected. When the dispersion effects are included from Eq. (11) one has to require that $E_l(l) > 0$ in the integrand of Eq. (8). Processes in which the undetected nucleon remains bound are beyond the scope of the present work and would require a proper quantum mechanical treatment to include its reabsorption vertex. At low energies this should be analyzed in terms of a proper optical potential model.

The results of Eq. (1) for the rescattering contributions leading to two nucleons in the continuum are plotted in Fig. 4. The yield resulting from rescattering is between one and two orders of magnitude smaller than the direct signal, except for low missing momenta and missing energies above 60 MeV, where it gives a correction of about 20%. The rescattering effects are also found to be independent on which of the above kinematics is chosen. For comparison we also show the results obtained by including only Pauli blocking and Fermi spreading and the ones obtained when the in-medium effects are included without requiring that the undetected nucleon is in the continuum [i.e., allowing $E_l(l) < 0$ in Eq. (8)]. Although the latter result has no direct physical relevance, it shows that only a part of the suppression of the rescattering effects is due to the corrections for effective mass in the medium ("m_D" curves of Fig. 4). The remaining reduction is a consequence of the energy required to reach the two-nucleon emission threshold.

B. Proton knock out from the SRC region

This section considers the results for the kinematics of Ref. [17], where the aim is to directly probe SRC. In this case it is convenient to write the spectral function as the sum of a mean field and a correlated part,
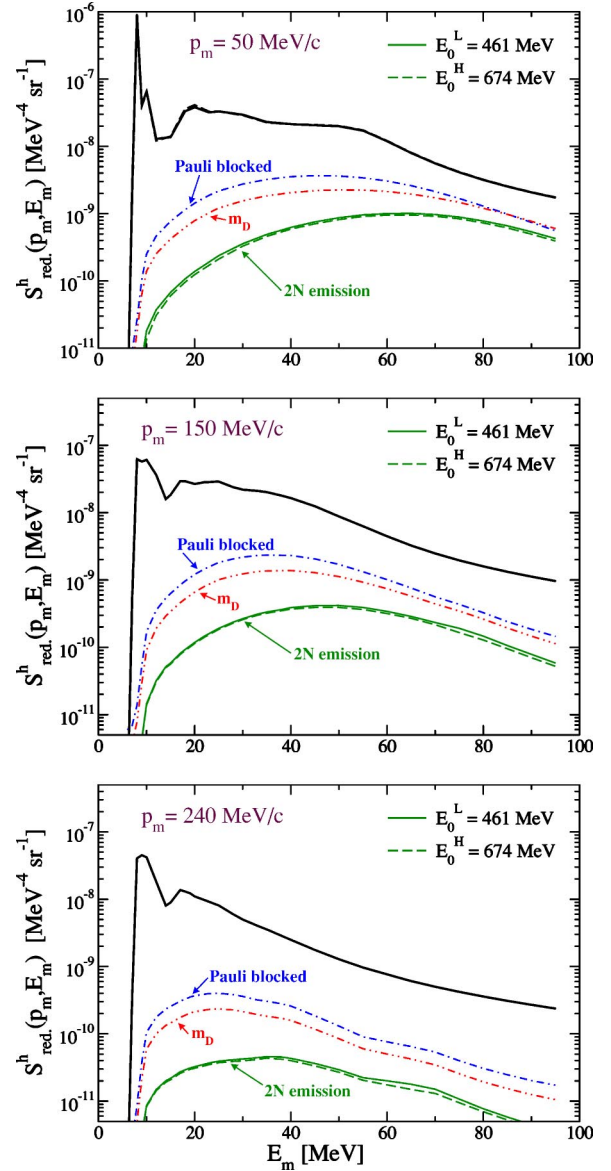

FIG. 4. (Color online) Theoretical results for the rescattering contribution to the reduced spectral strength of ^{208}Pb for the kinematics of Ref. [12]. The full (dashed) lines refer to the kinematics with lower (E_o^L) and higher (E_o^H) energy beams. The black lines shows the input spectral function, Eq. (13). The results obtained for rescattering with two nucleons emitted in the continuum are given by the green curves. For the kinematics E_o^L, the plots show the effects due only to Pauli blocking and Fermi spreading (dot-dashed lines). If the in medium dispersion was accounted for but no two-nucleon emission was imposed, Eq. (8) would give to the dot-dot-dashed curves.

$$S^h(p_m, E_m) = S_{MF}^h(p_m, E_m) + S_{corr}^h(p_m, E_m), \qquad (16)$$

where $S_{corr}^h(p_m, E_m)$ describes the short-range correlated tail at very high missing energies and momenta [3,7]. In the present work this was parametrized as
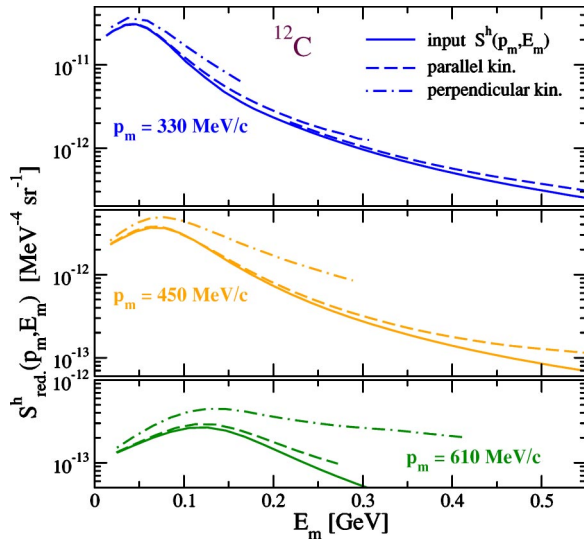
FIG. 5. (Color online) Theoretical results for the total (direct+rescattered) reduced spectral strength in the correlated region. The results are given for parallel (dashed line) and perpendicular kinematics (dot-dashed line). The full lines show the model spectral function, Eq. (16), employed in the calculations. All panels refer to a ^{12}C target and employ the same line convention. Note that the results for different sets of parallel kinematics do not always overlap exactly. This is mostly due to the dependence of the off-shell cross section σ_{eN}^{cc1} on the kinematics [16].

$$S_{corr}^{h}(p_m, E_m) = \frac{C\, e^{-\alpha p_m}}{[E_m - e(p_m)]^2 + [\Gamma(p_m)/2]^2}, \qquad (17)$$

where $e(p_m)$ and $\Gamma(p_m)$ are smooth functions of the missing momentum that were chosen to give an appropriate fit to the available ^{12}C$(e, e'p)$ data in parallel kinematics [8]. The solid line in Fig. 5 shows the model spectral function, Eq. (16), employed in the present calculations for that part of the p_m-E_m plane where S_{corr}^h dominates. The calculation with a ^{197}Au target employed the same S_{corr}^h of Eq. (17) multiplied by $79/6$ or $118/6$ to account for the correct number of protons and neutrons, respectively. This is shown for protons in Fig. 6. At energies close to the Fermi level the hole spectral function is dominated by its mean field component. For ^{12}C these are orbitals in the s and p shells, which are known experimentally and represent about 60% of the total strength. The spectroscopic factors and wave functions used in Eqs. (13)–(15) are the ones extracted from the world data in Ref. [38]. Since no direct data are available for gold we choose to employ the spectral function discussed above for the neighbor nucleus ^{208}Pb [12] but modifying the occupation of the last orbitals to account for the different number of nucleons in those shells.

We have performed calculations of the rescattering contributions by employing same sets of three parallel and two perpendicular kinematics used in Ref. [16]. In the parallel case, the initial momentum of the proton ($-\mathbf{p}_m$) was centered at different angles with respect to the momentum transferred by the electron, $\vartheta_{qpi} \sim 25$, 21, and 36 deg, while the corresponding energies of the final proton were centered at E_f
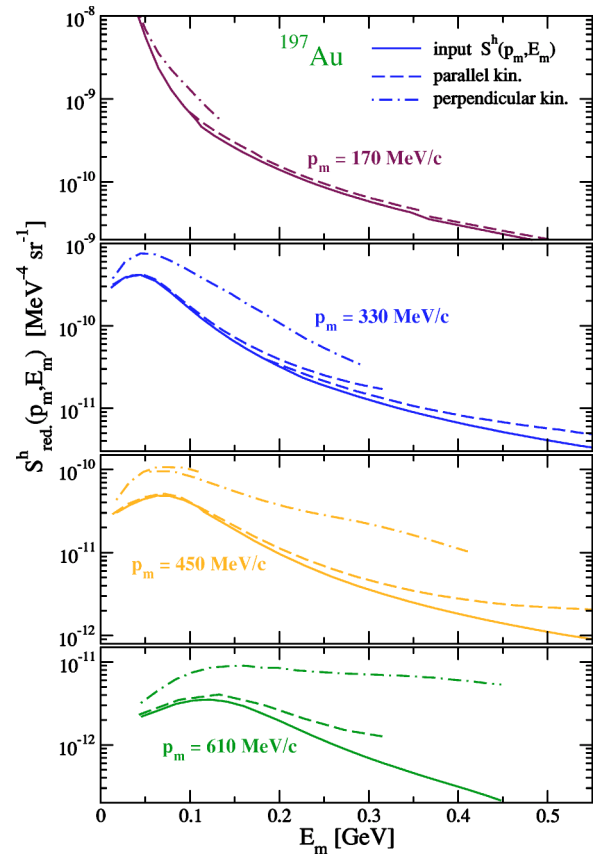

FIG. 6. (Color online) Theoretical results for the total reduced spectral strength in the correlated region. The results are given for parallel (dashed line) and perpendicular kinematics (dot-dashed line). The full lines show the model spectral function, Eq. (16), employed in the calculations. All panels refer to a ^{197}Au target and employ the same line convention. Note that the results for different sets of kinematics do not always overlap exactly. This is mostly due to the dependence of the off-shell cross section σ_{eN}^{cc1} on the kinematics [16].

~ 1.6, 1.8, and 1.9 GeV. This implied angles $\vartheta_{qf} \sim 0.5$, 1.5, and 10 deg, respectively, between the final proton and the momentum transferred. For the two perpendicular kinematics, the same angle $\vartheta_{qpi} \sim 90$ deg was used, while $E_f \sim 1.25$ and 1.35 GeV and $\vartheta_{qf} \sim 25$ and 29 deg. The four-momentum transferred by the electron was always in the range $Q^2 \sim 0.3 - 0.4$ GeV^2. More details on these kinematics are discussed in Ref. [16].

Due to the loss of energy of the ejected nucleon at the rescattering vertex, the spectral strength is always shifted toward higher missing energies. This is clearly visible in the results for both ^{12}C and ^{197}Au, which are shown in Figs. 5 and 6 (the sum of direct plus rescattering signals is plotted). The contribution to parallel kinematics is negligible at missing energies below the peak of the correlated tail but it tends to become more important for $E_m > 150 - 200$ MeV. This confirms the expected trend that a part of the strength seen in this region is dragged from places where the hole spectral function is larger [15]. The same behavior is seen in perpendicular kinematics, where, however, rescattering effects are already relevant at small missing energies. In this situation
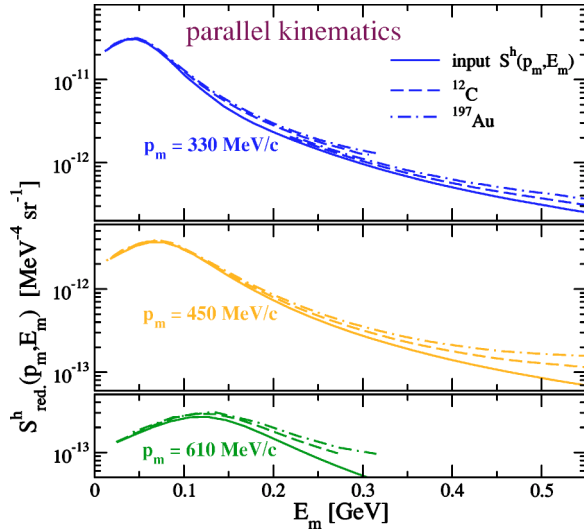
FIG. 7. (Color online) Theoretical results for the total reduced spectral strength of ^{12}C obtained in parallel kinematics (dashed line) compared to the analogous results for ^{197}Au (dot-dashed line), normalized to the number of protons of carbon. The full line shows the input spectral function of Eq. (16) employed in the calculations. All panels employ the same line convention.

the direct process accounts for only 30-50 % of the total yield obtained at the top of the correlated peak. At higher energies, the rescattering can overwhelm the PWIA signal by more than an order of magnitude. It should be noted that for both parallel and perpendicular kinematics the FSI become more important as the mass number increases. In general,
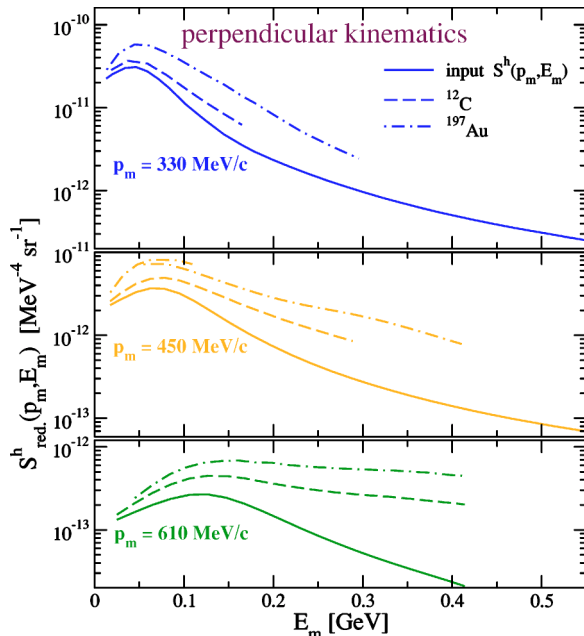

FIG. 8. (Color online) Theoretical results for the total reduced spectral strength of ^{12}C obtained in perpendicular kinematics (dashed line) compared to the analogous results for ^{197}Au (dot-dashed line), normalized to the number of protons of carbon. The full line shows the input spectral function of Eq. (16) employed in the calculations. All panels employ the same line convention.
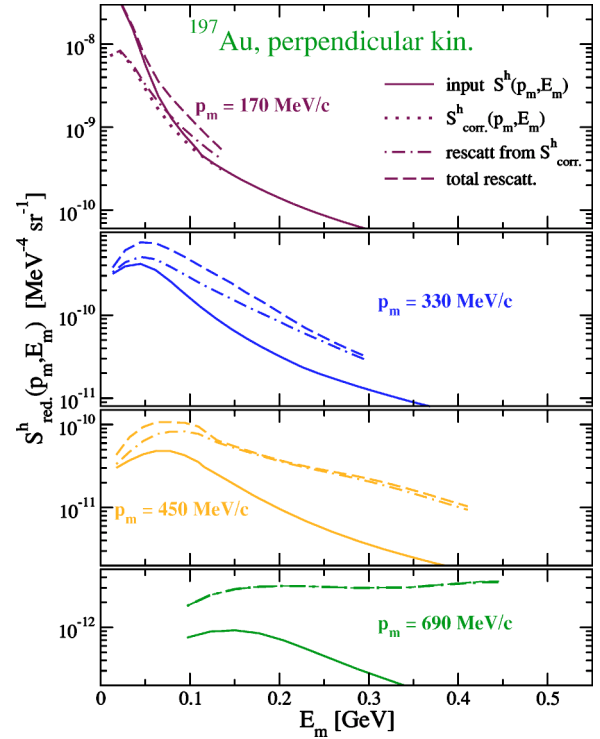

FIG. 9. (Color online) Reduced spectral strength of ^{197}Au computed in perpendicular kinematics as generated by the full spectral function of Eq. (16) (dashed line) or by the sole correlated part S^h_{corr} (dot-dashed line). The full line shows the model spectral function of Eq. (16). Its mean field component, S^h_{MF}, is not visible in this plot except for small missing momenta. Note that the dashed and dot-dashed lines overlap in the bottom panel. All panels employ the same line convention.

this is due to the average distance that the outgoing nucleon has to travel inside the nucleus. Thus it carries a dependence on the nuclear radius. Figure 7 compares the results for both target nuclei in parallel kinematics. For comparison the yield for ^{197}Au has been normalized to the same number of protons of ^{12}C. The reduced spectral function of gold is indeed always larger. The same consideration applies for perpendicular kinematics in Fig. 8.

To study the origin of the rescattered strength, the calculations were repeated for gold by neglecting the mean field orbitals, S^h_{MF}, in Eq. (16). For this nucleus the mean field strength extends to large missing energies, up to $\sim$100 MeV. Thus rescattering effects can easily spread it into the correlated region. Figure 9 compares the theoretical reduced spectral strength of Au in perpendicular kinematics with the analogous result obtained when S^h_{MF} is included. As one can see, relevant contributions from the mean field appear for momenta up to about 500 MeV/c. The results at higher missing momenta are completely dominated by the rescattering from the correlated tail S^h_{corr} into the correlated region itself. The situation is instead different in parallel kinematics where the present results for two-step rescattering do not shift any strength from the mean field region, even for a large nucleus like Au. Such a large shift appears to be energetically forbidden due to the large energy of the scattered proton adopted in these kinematics.

V. CONCLUSIONS

A proper understanding of the relevance of FSI and their dependence on the kinematics is important in modern $(e,e'p)$ experiments that attempt to observe the correlated strength at medium and high missing energies. The present work suggests a semiclassical approach to compute the effects of two-step rescattering, which is one of the leading contributions at high proton energies, and applies it to investigate its consequences for the kinematics of two different experiments.

The model assumes a PWIA for the electromagnetic vertex, in which the struck nucleon is described by the full hole spectral distribution of the target nucleus. This gives the possibility of investigating how FSI shift the original strength from the direct process within the missing energy and momentum plane. The absorption effects of the medium were accounted for by means of transparency factors. The rescattering is described in terms of the differential nucleon-nucleon cross section modified in order to account for Pauli blocking and Fermi spreading effects. The dispersion effects due to the nuclear medium have been included from DBHF results at the energies where they are relevant.

For kinematics involving outgoing protons of the order of few hundreds of MeV, the present model was employed to estimate the reappearance of strength through inelastic channels that lead to two-nucleon emission. In the reaction ^{208}Pb$(e,e'p)$ the overall effects were seen to be more than an order of magnitude smaller than the direct signal, slightly increasing for small missing momenta and missing energies above 60 MeV. This supports an analysis of the experimental data based on usual distorted wave calculations.

The same model was applied for the kinematics of the E97-006 experiment at Jefferson Laboratory that focused on the SRC distributions at high momenta. Calculations were performed for ^{12}C and ^{197}Au targets, which have different radii. In general, rescattering was found to be much smaller in parallel kinematics than in perpendicular ones. In the latter case a large amount of strength is shifted from regions where the spectral function is big to regions where it is smaller, thus overwhelming the experimental yield from the direct process. This confirms the studies of Ref. [15]. The contribution from rescattering effects is also seen to increase with the nuclear radius. The rescattering of nucleons originally emitted form the mean field orbitals was found to be important in perpendicular kinematics and for missing momenta lower than $\sim$500 MeV/c. No such large shift of strength was found in the parallel case. The remaining effects of rescattering are due to a rearrangement of the spectral strength within the correlated tail itself.

The present results provide a good first insight in the redistribution of strength due to FSI in $(e,e'p)$ reactions. However, it is clear that in order to properly explain the real experimental yield observed at high missing energies and for heavy nuclei other effects beyond the two-step rescattering need to be addressed [20,21]. Relevant extensions of the present formalism would include corrections from meson exchange and nucleon excitation processes, as well as an investigation of the importance of multiple rescattering for heavy nuclei in parallel kinematics. Work in this direction is in progress.

[1] V. R. Pandharipande, I. Sick, and P. K. A. deWitt Huberts, Rev. Mod. Phys. **69**, 981 (1997).

[2] W. H. Dickhoff and C. Barbieri, Prog. Part. Nucl. Phys. **52**, 377 (2004).

[3] H. Müther and W. H. Dickhoff, Phys. Rev. C **49**, R17 (1994); H. Müther, W. H. Dickhoff and A. Polls, *ibid.* **51**, 3040 (1995).

[4] S. C. Pieper, R. B. Wiringa, and V. R. Pandharipande Phys. Rev. C **46**, 1741 (1992).

[5] B. E. Vonderfecht, W. H. Dickhoff, A. Polls, and A. Ramos, Phys. Rev. C **44**, R1265 (1991).

[6] Y. Dewulf, W. H. Dickhoff, D. Van Neck, E. R. Stoddard, and M. Waroquier Phys. Rev. Lett. **90**, 152501 (2003).

[7] O. Benhar, A. Fabrocini, S. Fantoni, and I. Sick, Nucl. Phys. **A579** 493 (1994).

[8] T. Frick, Kh. S. A. Hassaneen, D. Rohe, and H. Müther, Phys. Rev. C **70**, 024309 (2004).

[9] L. Lapikás, Nucl. Phys. **A553**, 297c (1993)

[10] C. Barbieri and W. H. Dickhoff, Phys. Rev. C **65**, 064313 (2002).

[11] J. R. Terry, D. Bazin, B. A. Brown, J. Enders, T. Glasmacher, P. G. Hansen, B. M. Sherill, and J. A. Tostevin, Phys. Rev. C **69**, 054306 (2004).

[12] M. F. van Batenburg, Ph. D. Thesis, University of Utrecht, 2001.

[13] R. W. Lourie, *et al.*, Phys. Rev. Lett. **56**, 2364 (1986).

[14] H. Baghaei, *et al.*, Phys. Rev. C **39**, 177 (1989); L. B. Weinstein, *et al.*, Phys. Rev. Lett. **64**, 1646 (1990).

[15] I. Sick, *et al.*, JLab Proposal E97-006 (1997).

[16] D. Rohe, Eur. Phys. J. A **A17**, 439 (2003) (conference proceeding on Electron-Nucleus Scattering VII in Elba 2002); D. Rohe, Habilitationsschrift, University of Basel, 2004 (unpublished).

[17] D. Rohe, *et al.*, Phys. Rev. Lett. (to be published); nucl-ex/0405028.

[18] D. Knödler and H. Müther, Phys. Rev. C **63**, 044602 (2001).

[19] P. Demetriou, S. Boffi, C. Giusti, and F. D. Pacati, Nucl. Phys. **A625**, 513 (1997).

[20] N. Nikolaev, A. Szczurek, J. Speth, J. Wambach, B. G. Zakharov, and V. R. Zoller, Nucl. Phys. **A582**, 665 (1995).

[21] H. Morita, C. Ciofi degli Atti, and T. Treleani, Phys. Rev. C **60**, 034603 (1999).

[22] J. Ryckebusch, D. Debruyne, P. Lava, S. Janssen, B. Van Overmeire, and T. Van Cauteren, Nucl. Phys. **A728**, 226 (2003).

[23] V. R. Pandharipande and S C. Pieper, Phys. Rev. C **45**, 791 (1992).

[24] T. de Forest, Jr., Nucl. Phys. **A392**, 232 (1983).

[25] R. Schiavilla, D. S. Lewart, V. R. Pandharipande, S. C. Pieper, R. B. Wiringa, and S. Fantoni, Nucl. Phys. **A473**, 267 (1987).

[26] H. de Vries, C. W. de Jager, and C. de Vries, At. Data Nucl. Data Tables **36**, 495 (1987).

[27] S C. Pieper (private communication).

[28] J. J. Kelly, Phys. Rev. C **54**, 2547 (1996).

[29] M. E. Peskin and D. V. Schroeder, *An Introduction to Quantum Field Theory* (Perseus, Reading, Mass., 1995).

[30] R. A. Arndt, I. I. Strakovsky, and R. L. Workman, Phys. Rev. C **62**, 034005 (2000); SAID database web site: http://gwdac.phys.gwu.edu.

[31] K. Hagiwara, *et al.*, Phys. Rev. D **66**, 010001 (2002); particle data group web site http://pdg.bnl.gov.

[32] B. D. Serot and J. D. Walecka, Adv. Nucl. Phys. **16**, 1 (1986).

[33] R. Brockmann and R. Machleidt, Phys. Rev. C **42**, 1965 (1990).

[34] G. Q. Li and R. Machleidt, Phys. Rev. C **48**, 1702 (1993); **49**, 566 (1994).

[35] C. Fuchs, A. Faessler, and M. El-Shabshiry, Phys. Rev. C **64**, 024003 (2001).

[36] M. Jaminon and C. Mahaux, Phys. Rev. C **40**, 354 (1989).

[37] G. E. Brown and M. Rho, Nucl. Phys. **A732**, 397 (1981).

[38] L. Lapikás, G. van der Steenhoven, L. Frankfurt, M. Strikman, and M. Zhalov, Phys. Rev. C **61**, 064325 (2000).